Green Emission in Thermally Stable Er^{3+} Doped Lead-Free Perovskite Phosphor for Solid-State Lighting and Optical Thermometry Applications

Ishant Kumar, Avinash Kumar, Sandeep Kumar, Vikas Sangwan, and Arvind K. Gathania

***Abstract*—$CaTiO_3$:xEr^{3+} (0.1≤x≤7 mole%) phosphor materials were meticulously prepared through the solution combustion method. Comprehensive analyses employing Powder X-ray Diffraction (PXRD), Field Emission Scanning Electron Microscopy (FESEM), and Fourier Transform Infrared Spectroscopy (FTIR) were conducted to investigate the phase, morphology, and vibrational characteristics of the synthesized phosphors. A detailed luminescence study was undertaken using photoluminescence spectroscopy, revealing distinctive 4f-4f transitions associated with Er^{3+} in both excitation and emission spectra. The application of Dexter's theory provided insights into the quenching mechanism inherent in $CaTiO_3$:Er^{3+} phosphors. Photometric studies were carried out to evaluate the suitability of the synthesized material for solid-state lighting applications. Furthermore, to assess the thermal stability of the phosphor material, the activation energy was computed. The fluorescence intensity ratio of thermally coupled energy levels of Er^{3+} ion was utilized to assess the temperature-sensing capabilities of the synthesized material. This material may be suitable for solid-state lighting and optical thermometry applications.**

***Index Terms*—Perovskite, phosphor, solid-state lighting, and optical thermometry.**

I. Introduction

LUMINESCENT materials, commonly denoted as phosphor materials, constitute inorganic compounds deliberately infused with impurities such as rare earth and transition metal ions. Solid-state lasers, optical temperature sensors, field emission displays, plasma display panels, and solid-state lighting exemplify a diverse array of applications associated with phosphors [1], [2], [3], [4], [5]. The versatility and efficacy of these materials make them integral components in a spectrum of cutting-edge technologies. From precise laser systems to highly sensitive temperature monitoring devices, and from state-of-the-art display technologies to innovative lighting solutions, the multifaceted utility of these materials underscores their significance in various industries [6], [7], [8], [9]. Conventional lighting sources, such as incandescent and fluorescent lights, constitute a significant portion of global electricity consumption, exceeding one-fourth of the total energy used worldwide. In response to this considerable challenge, material scientists have dedicated substantial efforts to replace these traditional sources with energy-efficient solid-state lighting alternatives. White light-emitting diodes (WLEDs) incorporating phosphor conversion present a particularly advantageous solution for energy conservation [10], [11]. Commercially, WLEDs are typically fabricated using an InGaN blue chip and Ce^{3+} yellow phosphor [12]. However, this production method falls short of meeting the criteria for high-quality interior illumination due to the absence of a red-light component in the overall emission. This results in an elevated correlated color temperature (CCT) of WLEDs and a correspondingly diminished color rendering index. To meet the standards of superior lighting quality, WLEDs must exhibit a lower correlated color temperature for indoor lighting applications and demonstrate an enhanced color rendering index [13], [14]. Achieving these characteristics is paramount to ensuring optimal visual comfort, color fidelity, and overall lighting performance in diverse applications ranging from commercial and residential settings to industrial environments. Consequently, researchers adopted an alternative strategy to enhance the quality of WLEDs by encapsulating a Near-Ultraviolet (NUV) blue chip with a composite of red, green, and blue phosphors [15], [16]. The identification of green, red, and blue phosphors responsive to NUV light becomes paramount in this context. Thus, our focus centres on the development of a novel green phosphor to serve as a color-mixing element for phosphor-converted WLEDs utilizing NUV chips.

Temperature constitutes a fundamental physical parameter across various domains of natural science, encompassing biological systems, industrial processes, and scientific investigations. Consequently, precise temperature monitoring assumes paramount importance in numerous aspects of life. Contact thermometers, relying on the thermal expansion of liquids and metals, serve as conventional instruments for direct temperature measurement through physical contact with the target object. Nonetheless, a limitation of these sensors lies in their inability to gauge the temperature of inaccessible entities, such as

Manuscript received 16 March 2024; revised 15 April 2024; accepted 17 April 2024. Date of publication 23 April 2024; date of current version 2 May 2024. *(Corresponding author: Arvind K. Gathania.)*

Ishant Kumar is with the Department of Physics and Photonics Science, National Institute of Technology, Hamirpur 177005, India, and also with the Department of Physics, Rabindranath Tagore Government College, Sarkaghat District, Mandi 175024, India.

Avinash Kumar, Sandeep Kumar, and Arvind K. Gathania are with the Department of Physics and Photonics Science, National Institute of Technology, Hamirpur 177005, India (e-mail: akgathania@nith.ac.in).

Vikas Sangwan is with the Department of Applied Physics, Delhi Technological University, Delhi 110 042, India.

Digital Object Identifier 10.1109/JPHOT.2024.3392566

those found in high-voltage power plants, oil refineries, coal mines, high-pressure power plants, and corrosive environments. Consequently, achieving precise temperature measurements remains a focal point for scientific researchers. To surmount the shortcomings of traditional contact thermometers, non-contact optical thermometry has garnered considerable interest among the scientific community. This attention is attributable to the fact that temperature profoundly influences fluorescence intensity, a pivotal characteristic of luminescent materials [17]. Due to its advantageous attributes, encompassing elevated sensitivity, precise spatial resolution, rapid response times, and the capability for real-time monitoring, the Fluorescence Intensity Ratio (FIR) method has garnered substantial research attention. This method is based on the examination of emissions from rare earth ion's thermally related energy levels, with a particular emphasis on the intensity ratio that varies with temperature [18], [19], [20], [21]. This feature endows it with suitability for the accurate temperature detection of typically inaccessible objects. Specifically, certain rare earth ions namely Er^{3+}, Ho^{3+}, Tm^{3+}, and Nd^{3+}- manifest pairs of thermally coupled energy levels, rendering them particularly well-suited for application in FIR based optical thermometers [22], [23], [24], [25], [26], [27]. The design and development of a phosphor material for an optical temperature sensor necessitate careful consideration of two primary factors. Firstly, the selection of an optically active ion capable of modulating its emission in response to temperature is crucial. Secondly, the choice of a host matrix assumes significance, as it profoundly influences the temperature-sensing capabilities and emission intensity of the phosphor material. In creating phosphor materials for optical temperature sensors, it's best to choose host matrices that are stable physically and chemically, have low phonon energy, and wide band gap [28]. Numerous phosphors, like $PbLa_{2-2x}Eu_{2x}W_4O_{16}$ [29] $CsPbCl_3$:Bi^{3+}, Eu^{3+} [30], $PbZrTiO_3$:Er^{3+},Yb^{3+} [31] etc. incorporate lead, a substance known for its deleterious impact on both human health and the environment due to its toxic radiation effects [32]. Considering these considerations, a collaborative endeavour has been undertaken to investigate alternative materials with environmentally sustainable attributes, serving as replacements for lead-based counterparts. The intricate oxide $CaTiO_3$ has been chosen as the host matrix in our study due to its non-toxic nature, commendable chemical and thermal stability, and relatively low phonon energy of approximately 470 cm^{-1} [33]. The orthorhombic structure of $CaTiO_3$ classifies it within the perovskite family, characterized by the generic chemical formula ABO_3. Here, B represents a cation featuring a relatively small ionic radius, exemplified by Ti^{4+}, while A denotes a cation with a larger ionic radius, exemplified by Ca^{2+}. The crystal structure of $CaTiO_3$ incorporates CaO_8 polyhedra and TiO_6 octahedra [34]. Possessing a notable band gap of 3.5 eV, $CaTiO_3$ stands out as one of the preeminent wide band gap oxides [35], [36]. Researchers have widely adopted $CaTiO_3$ as a host matrix for the formulation and advancement of rare earth-doped nano phosphors due to their distinctive attributes. These include elevated luminous efficiency, minimal phonon energy, a broadband gap, facile synthetic conditions, environmental compatibility, and robust thermal and chemical stability [37]. There has been considerable exploration of rare earth doped $CaTiO_3$ to enhance its luminescent properties, showcasing its applicability across various industrial domains [38], [39]. A key rationale for selecting Er^{3+} ions as dopants resides in their distinct energy levels, specifically $^2H_{11/2}$ and $^4S_{3/2}$, which exhibit thermal coupling and yield green light emission. This characteristic renders Er^{3+} ions particularly advantageous for applications spanning optical thermometry and the development of nano phosphors emitting green light [7].

While up conversion phosphor-based optical thermometers have been extensively scrutinized and find application in diverse fields, the competitive advantages offered by down-converting nano phosphors warrant a more comprehensive investigation for optical thermometer design. In the current study, we delve into the bifunctional attributes of $CaTiO_3$ doped with Er^{3+} ions, specifically focusing on its capabilities in temperature sensing and solid-state lighting. To the best of our knowledge, the temperature-dependent down-conversion behaviour of $CaTiO_3$:Er^{3+} has not been systematically explored. Our research is dedicated to elucidating the down-conversion characteristics of the $CaTiO_3$:Er^{3+} phosphor in relation to temperature variations, to establish its suitability as an optimal candidate for optical thermometry applications.

This study explores the dual applications of Er^{3+} doped phosphor, specifically focusing on solid-state illumination and optical thermometry. The solution combustion method was utilized to synthesize Er^{3+} doped phosphors due to its numerous benefits, including cost-effectiveness, time efficiency, and environmentally friendly nature [40]. The resulting material demonstrates commendable color purity, good thermal stability, and high sensitivity, indicating promising prospects for applications in solid-state lighting and optical thermometry.

II. Experimental

A. Phosphor Preparation

The preparation of a series of $CaTiO_3$:x Er^{3+} ($0.1 \leq x \leq 7$ mole%) phosphors using the solution combustion method involved several steps. Analytical reagent grade $Ti(OCH_2CH_2CH_2CH_3)_4$, HNO_3 (70%), $Ca(NO_3)_2 \cdot 4H_2O$, $Er(NO_3)_3 \cdot 5H_2O$, and NH_2CONH_2 were the starting materials. The synthesis process initiated with the preparation of a titanium nitrate solution. In a 100 ml beaker, 10 ml of double-distilled water and 1-2 ml of HNO_3 were added to $Ti(OCH_2CH_2CH_2CH_3)_4$. The mixture was agitated on a magnetic stirrer until a clear solution of titanium nitrate was obtained. Subsequently, stoichiometric quantities of nitrates of calcium, erbium, and urea were incorporated into the titanium nitrate solution. The resulting mixture was continuously stirred on a magnetic stirrer at an elevated temperature of approximately 80–90 °C until it transformed into a dense slurry. The obtained slurry was then subjected to a furnace heated to 500 °C to produce a fluffy powder. To enhance the crystallinity of the phosphor powder, it underwent annealing at 800 °C for a duration of 2 h. This multi-step process aimed at the preparation of high-quality phosphors for further applications.

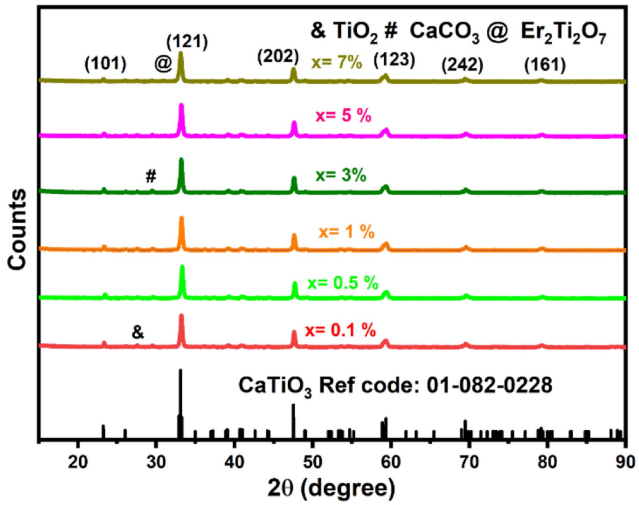

Fig. 1. PXRD patterns of $CaTiO_3$:x Er^{3+} (0.1≤x≤7 mole%).

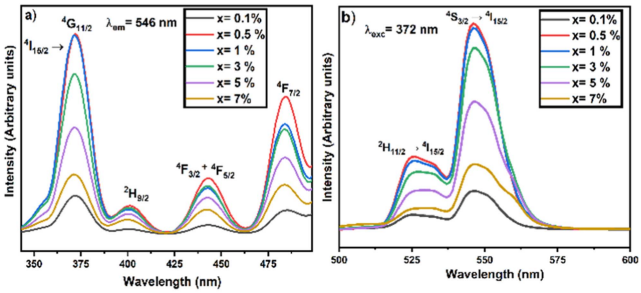

Fig. 2. (a) Excitation and (b) emission spectra of $CaTiO_3$:x Er^{3+} (0.1≤x≤7 mole%).

B. Characterization

The characterization performed in the present manuscript is same as reported in our earlier work [7], [28] and their details can be found from there.

III. Results and Discussions

A. PXRD Study

Fig. 1 presents the powder X-ray Diffraction (PXRD) pattern of $CaTiO_3$:xEr^{3+} (0.1≤x≤7 mole%) phosphor. The PXRD patterns of all the samples matches closely with the diffraction patterns of $CaTiO_3$ with ICSD (Inorganic crystal structure database) Reference Code 01-082-0228. $CaTiO_3$:xEr^{3+} (0.1≤x≤7 mole%) crystallizes into orthorhombic phase with space group Pbnm [34]. Most intense diffraction peaks of the phosphor are effectively indexed to (101), (121), (202), and (123) (242) (161). The average crystallite size was determined using Scherer's formula [41]:

$$D = \frac{K\lambda}{\beta \mathrm{Cos}\,\theta} \quad (1)$$

where 'D' represents the average crystalline size, λ is the X-ray wavelength (1.54056 Å), K is a constant, θ is the Bragg's angle, and β is the full width at half maximum (FWHM). The calculated crystallite size falls within the range of 19–22 nm. Small impurity reflections marked by ampersand (&), hash (#), and at the rate of (@) were also observed due to presence of TiO_2, $CaCO_3$ and $Er_2Ti_2O_7$ phases.

The Rietveld refinement analysis of $CaTiO_3$:xEr^{3+} (0.1≤x≤7 mole%) was performed on major phase ($CaTiO_3$) using the FULLPROF suite program. The Pseudo-Voigt function was employed to fit various parameters of the data points. Fig. S1 illustrates the Rietveld refinement of the XRD patterns of $CaTiO_3$:xEr^{3+} (0.1≤x≤7 mole%). The detailed information about the various structural parameters evaluated from the Rietveld refinement analysis of various samples is presented in Table S1.

B. FESEM Study

Fig. S2 present high-magnification Field Emission Scanning Electron Microscopy (FESEM) images, detailing the morphological characteristics of $CaTiO_3$:0.5 mole% Er^{3+}. The FESEM images depict irregularly agglomerated distorted spherical-like particles. The particle distribution, as illustrated in the histogram within Fig. S2(a), reveals a predominant particle size clustering within the range of 20-100 nm. The average particle size is 55 nm. Further insight into the elemental composition was provided by the Energy Dispersive X-ray Spectroscopy (EDS) spectra, displayed in Fig. S2(b), affirming the presence of Ca, Ti, O, and Er within the $CaTiO_3$:0.5 mole% Er^{3+} phosphors.

C. FTIR Study

The investigation into the vibrational bands of $CaTiO_3$:x Er^{3+} at varying concentrations (x = 0.1–7 mol%), was conducted through Fourier Transform Infrared (FT-IR) studies, as depicted in Fig. S3. The peaks observed at 434 cm^{-1} and broadband from 525–745 cm^{-1} correspond to the stretching vibrations of Ti–O and the bridge stretching modes of Ti–O–Ti, respectively. These spectral features reflect the structural characteristics associated with the environment surrounding the TiO_6 octahedra in the ABO_3 perovskite [42]. The shoulder peak at 875 cm^{-1} appears due to the presence of out of plane bending of CO_3^{2-} ion present in $CaCO_3$ [43], [44]. Furthermore, the band at 1442 cm^{-1} was ascribed to the asymmetric stretching vibration of the CO_3^{2-} group present in $CaCO_3$ [45], [46].

D. Room Temperature Photoluminescence Study

Photoluminescence excitation and emission spectra at room temperature were systematically recorded to analyze the impact of doping on the luminescence characteristics of $CaTiO_3$:Er^{3+}. The Photoluminescence Excitation (PLE) and Photoluminescence (PL) spectra of $CaTiO_3$:Er^{3+} are illustrated in Fig. 2(a) and (b), respectively. The PLE spectra were acquired within the range of 300–500 nm, with the emission wavelength fixed at 546 nm. In line with our previous investigations, the PLE of Er^{3+} doped $CaTiO_3$ manifested multiple narrow bands between 350 and 500 nm, corresponding to distinct 4f electronic transitions of Er^{3+} ions. Notably, sharp bands at 372, 401 nm, 442, and 484

nm denote $^4I_{15/2} \rightarrow {}^4G_{11/2}$, $^4I_{15/2} \rightarrow {}^2H_{9/2}$, $^4I_{15/2} \rightarrow {}^4F_{3/2} + {}^4F_{5/2}$, and $^4I_{15/2} \rightarrow {}^4F_{7/2}$ transitions of Er^{3+} ions, respectively [7], [47]. For the analysis of PL properties, emission spectra were recorded at 372 nm excitation for all synthesized samples. The emission spectra exhibits characteristic green emission with peaks centred at 526 nm and 546 nm, corresponding to $^2H_{11/2} \rightarrow {}^4I_{15/2}$ and $^4S_{3/2} \rightarrow {}^4I_{15/2}$ transitions [22], [48]. Notably, there was no change in peak profile with variation in doping concentration. The partial energy diagram illustrating various excitation and emission profiles are presented in Fig. S4 (a). With an increase in doping amount, there was a rise in emission intensity up to 0.5 mole percentage, attributed to the increased luminescence centres. However, beyond 0.5 mole percentage, a decline in emission intensity occurred due to concentration quenching.

When the spatial separation between activators exceeds a specific threshold, an escalation in non-radiative transitions occurs. This phenomenon is attributed to the presence of cross-relaxation channels, which act as inhibitory sites. The activation of cross-relaxation channels occurs in energy levels with comparable energy differences between them. In the context of an energy transfer process, such as A + B → C + D, cross-relaxation channels become feasible if the energy difference between A and C closely matches the energy difference between B and D. Various cross-relaxation channels may be accountable for the heightened non-radiative transitions in the synthesized phosphors, and these are detailed below [7]:

$$\text{CRC1: } {}^2H_{11/2}(\text{Er1}) + {}^4I_{15/2}(\text{Er2}) \rightarrow {}^4I_{13/2}(\text{Er1}) + {}^4I_{9/2}(\text{Er2}) \quad (2)$$

$$\text{CRC2: } {}^4S_{3/2}(\text{Er1}) + {}^4I_{15/2}(\text{Er2}) \rightarrow {}^4I_{9/2}(\text{Er1}) + {}^4I_{13/2}(\text{Er2}). \quad (3)$$

Within CRC1, the Erbium ion in the excited state $^2H_{11/2}$ undergoes relaxation to the energy state $^4I_{13/2}$, subsequently transferring the remaining energy to an adjacent Erbium ion. As depicted in Fig. S4 (b), this energy transfer through CRC1 induces stimulation of a neighbouring Erbium ion in the ground state $^4I_{15/2}$ to the excited state $^4I_{9/2}$ level. In CRC2, the Erbium ion initially in the excited state $^4S_{3/2}$ undergoes relaxation to the $^4I_{9/2}$ state and transfers the remaining energy to another Erbium ion upon being excited from the ground state $^4I_{15/2}$ to the higher state $^4I_{13/2}$. These cross-relaxation channels contribute to the increase in non-radiative transitions, and similar channels have been observed in our previous work [7], confirming their role in the concentration quenching. The influence of exchange interaction is prominent when the critical distance (R_c) between adjacent activator ions is less than 5 Å, whereas distance exceeding 5 Å lead to multipole interactions. According to Blasses, the distance between adjacent Er^{3+} ions can be determined using the equation [49]:

$$R_c = 2\left[\frac{3V}{4\pi Z X_c}\right]^{\frac{1}{3}}. \quad (4)$$

Here, R_c represents the critical distance, V denotes the unit cell volume, X_c represents the critical concentration, and Z represents the number of sites available for dopant ion occupancy per unit cell in the host lattice. For the $CaTiO_3$ host with Z equal to 4, V equal to 224.241 $Å^3$, and X_c equal to 0.005, the calculated critical distance for energy transfer is 27.78 Å. Given that this value exceeds 5 Å, it indicates the prevalence of multipole-multipole interactions in $CaTiO_3$:Er^{3+}. The determination of multipole interactions can be carried out using the Dexter formula for energy transfer [50]:

$$\frac{I}{X} = k\left[1 + l(X)^{\frac{m}{3}}\right]^{-1}. \quad (5)$$

Here, I denotes PL intensity, and k and l are arbitrary constants, while X denotes the critical concentration. The value of m signifies the type of multipolar interaction, with various constant values corresponding to different types of multipolar interactions. Specifically, for values of m = 3, 6, 8, and 10, exchange interactions, dipole-dipole, dipole-quadrupole, and quadrupole-quadrupole interactions occur, respectively. The determination of the m value involves calculating it from the slope (m/3) of the graph log(I/X) vs log(X), as illustrated in Fig. S5. The computed value of m is 5.28, closely aligning with 6. This proximity implies that dipole-dipole interactions predominate in the synthesized phosphor.

E. Photometric Analysis

The determination of CIE (Commission Internationale de L'Eclairage) coordinates for the $CaTiO_3$:x Er^{3+} ($0.1 \leq x \leq 7$ mole%) phosphors followed the 1931 CIE standard. The CIE diagram, corresponding to an excitation wavelength of 372 nm, is depicted in Fig. S6, with the corresponding estimated values detailed in Table S2 (The CIE coordinates for different samples are indicated numerically, corresponding to the serial numbers listed in Table S2). The CIE coordinates of the optimized phosphor, $CaTiO_3$:0.5%Er^{3+}, were found to be (0.28195, 0.70117). It has been documented that a correlated color temperature (CCT) below 5000 K is suitable for warm white light used for inside home application whereas CCT value greater than 5000 K value is suitable for outside lighting applications [51]. Furthermore, color purity, an essential parameter WLED application. The CCT and color purity values of all the samples have been evaluated using the formula described in our previous work [7] and enlisted in Table S2. The high color purity and CCT (>5000 K) value indicates that synthesized phosphor can be used as cool green emitting phosphor for outside lighting applications.

F. Decay Curve

The decay characteristics of $CaTiO_3$:0.5% Er^{3+} phosphor was analysed, as depicted in Fig. S7. Remarkably, the decay behavior of $CaTiO_3$: 0.5% Er^{3+} phosphor is effectively described by a third-order exponential decay model (Exp Dec 3). The governing equation for Exp Dec 3 is denoted as equation (6) [52]:

$$I(t) = I_0 + A_1 e^{\frac{-t}{\tau_1}} + A_2 e^{\frac{-t}{\tau_2}} + A_3 e^{\frac{-t}{\tau_3}} \quad (6)$$

Here, A_1, A_2, and A_3 are constants, while I and I_0 are luminescent intensity at time t and initial time respectively. τ_1, τ_2, and τ_3 signify decay times. For $CaTiO_3$:Er^{3+}, specific decay

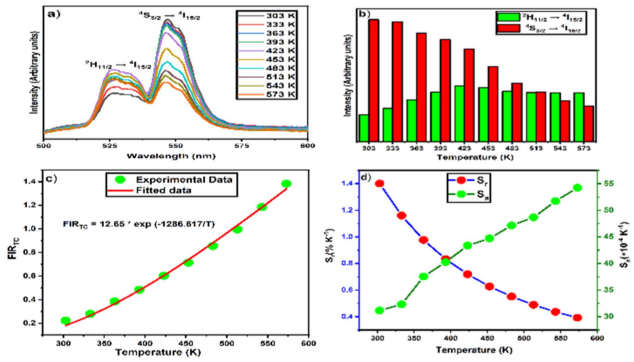

Fig. 3. Thermal evolution of (a) PL emission spectra of $CaTiO_3$: 0.5% Er^{3+} phosphor under 372 nm excitation (b) thermally coupled levels of Er^{3+} ion (c) FIR of thermally coupled levels of Er^{3+} ion and their fitting using Boltzmann's relation (d) relative and absolute sensitivity.

parameters were determined as follows: $A_1 = 0.72824$, $A_2 = 0.26383$, $A_3 = 0.33172$, $\tau_1 = 2.00036\ \mu s$, $\tau_2 = 15.39955\ \mu s$, and $\tau_2 = 76.42103\ \mu s$. The average lifetime value for the $CaTiO_3$:Er^{3+} phosphor was computed utilizing equation (7):

$$\tau_{av} = \frac{\sum A_i \tau_i^2}{\sum A_i \tau_i} \tag{7}$$

where, τ_{av}, τ_i, and A_i represent average lifetime, decay times, and constants. Through these calculations, the average lifetime was determined to be approximately 64.88 μs.

G. Thermal Stability

The influence of temperature on the PL characteristics of phosphor-based materials is a significant consideration for phosphor usage in numerous kinds of solid-state lighting applications. Usually, phosphors employed in illuminating devices necessitate excellent thermal stability as blue/UV LED chips generate temperatures of 150 °C during functioning time. Furthermore, the thermal quenching properties of the versatile phosphor are also beneficial for optical thermal sensing applications. By analyzing the emission profiles at varying temperatures, the thermal quenching features of the phosphor have been explored. The emission spectral profiles of the synthesized phosphor at 372 nm excitation as the temperature increased from 303 to 573 K, are illustrated in Fig. 3(a). The peak intensities of emission were dependent on temperature and the peak intensities associated with the transitions $^2H_{11/2} \rightarrow {}^4I_{15/2}$ and $^4S_{3/2} \rightarrow {}^4I_{15/2}$ vary with temperature. The emission peak related to the $^2H_{11/2} \rightarrow {}^4I_{15/2}$ transition at 526 nm increases with an upsurge in temperatures. Simultaneously, the emission peak at 546 nm is linked to the $^4S_{3/2} \rightarrow {}^4I_{15/2}$ transition, which diminishes with temperature. The $^2H_{11/2}$ energy level was thermally populated from the $^4S_{3/2}$ energy level via external temperature, which resulted in an intensity improvement in the $^2H_{11/2} \rightarrow {}^4I_{15/2}$ transition. This kind of variation in the PL spectral profiles occurs because of the thermally coupled and very little energy difference among the $^2H_{11/2}$ and $^4S_{3/2}$ energy levels of the dopant (Er^{3+}) ions. Furthermore, one of the most essential criteria of thermal stability for the synthesized phosphor is the activation energy, which was determined using the Arrhenius equation as shown below [53]:

$$I_T = \frac{I_0}{1 + Cexp\left(-\frac{\Delta E}{K_B T}\right)}. \tag{8}$$

The emission intensities at specific temperature T (K) and initial temperature are denoted as I_T and I_0. The Boltzmann and arbitrary constant parameters are represented as K_B and C. The activation energy of the phosphor is noted ΔE. The Arrhenius equation has been applied to assess the ΔE based on the slope of a straight line between $\ln[(I_0/I_T) - 1]$ and $1/K_BT$. The slope value was determined to be 0.279, as shown in Fig. S8. For the synthesized phosphor, ΔE is found to be 0.279 eV. Henceforth, the influence of temperature on the emission profiles of the synthesized phosphor indicates that the phosphor has excellent thermal stability.

H. Thermal Sensing

Fig. 3(a) present the thermal evolution of the emission profile of phosphor excited by 372 nm excitation within the temperature range of 303–573 K. The variation in CIE coordinates with T is negligible as depicted in Fig. S9. The emission intensity at 526 nm is observed to escalate relative to the emission at 546 nm with increasing temperature, as depicted in Fig. 3(b). This phenomenon emerges due to the thermal interconnection between two emitting levels. The relative population of these thermally coupled energy levels, separated by thermal energy (of the order of K_BT), conforms to a Boltzmann-type distribution. This distribution significantly influences the transitions between the two levels, particularly at elevated temperatures. The FIR associated with the thermally coupled levels can be described by the following expression [54]:

$$FIR_{TC} = \frac{I_{526}}{I_{546}} = A\, e^{\left(\frac{-\Delta E}{K_B T}\right)} \tag{9}$$

where I_{526} and I_{546} represent the integrated emission intensity of two thermally coupled (TC) green emitting bands, ΔE represents the energy difference between two TC levels. K_B, T, and A represent Boltzmann's constant, absolute temperature, and constant in relation to degeneracy, spontaneous radiative transition rate, and angular frequency of the respected transition. In Fig. 3(c), the experimentally determined FIR values are presented against temperature (T). The FIR data is fitted using the Boltzmann formula, and the value of $\Delta E/K_B$ is derived from the gradient of the fitted formula. Additionally, ΔE is determined to be approximately 894.25 cm^{-1}. By analysing emission spectra, the value of ΔE is found to be 696.39 cm^{-1}. The presence of non-radiative cross-relaxation channels and the overlap of two thermally coupled energy levels account for the observed subtle energy differential of 197.86 cm^{-1} [54]. In optical temperature-sensing, certain performance parameters like relative and absolute sensitivity are crucial for comparing

various optical temperatures. The absolute and relative sensitivities are defined as [55], [56]:

$$S_a = \left|\frac{d\left(FIR_{TC}\right)}{dT}\right| = \left|\frac{\Delta E}{K_B T^2} \times FIR_{TC}\right| \quad (10)$$

$$S_r = \left|\frac{1}{FIR_{TC}} \times \frac{d\left(FIR_{TC}\right)}{dT}\right| = \left|\frac{\Delta E}{K_B T^2}\right|. \quad (11)$$

The temperature-dependent behaviour of S_a and S_r is evident in Fig. 3(d), showing a steady increase with temperature. At 573 K, S_a attains its peak value, reaching 54.23 $\times$ 10^{-4}% K^{-1}. Conversely, S_r displays a consistent decreasing pattern with temperature, with its maximal value of 1.40% K^{-1} recorded at 303 K. A comparative analysis of S_a and S_r with other temperature sensing phosphors is enlisted in Table S3.

IV. Conclusion

In the current work, Er^{3+} doped $CaTiO_3$ has been successfully synthesized through solution combustion method. The obtained material underwent structural confirmation and morphology analysis via Powder X-ray Diffraction (PXRD) and Field Emission Scanning Electron Microscopy (FESEM), respectively. Additionally, Fourier Transform Infrared Spectroscopy (FTIR) was employed for vibrational characterization. Photoluminescence (PL) emission spectra were recorded at an excitation wavelength of 372 nm, revealing a distinctive green emission attributable to specific transitions. Notably, our investigation indicates a notable increase in PL emission with the initial rise in Er^{3+} concentration. However, beyond a critical concentration (x = 0.5 mol%), there is a discernible decline in emission intensity. Dexter theory elucidates that dipole-dipole interactions play a pivotal role in the observed quenching phenomenon. Calorimetric analysis of the material yields CIE coordinates, CCT, and color purity values, denoting its suitability as a green component in solid-state lighting applications. Given the thermal coupling of transitions, our study delves into potential applications, revealing the synthesized material's efficacy in optical thermometry. Maximum relative sensitivity of 1.40% K^{-1} and absolute sensitivity of 54.23 $\times$ 10^{-4}% K^{-1} were observed at temperatures of 303 K and 573 K, respectively. In summary, our findings underscore the multifunctional potential of the synthesized material. It exhibits promise for applications in both solid-state lighting and non-contact optical thermometry, establishing its viability as a bifunctional material with diverse practical implications.

References

[1] H. Scheife, G. Huber, E. Heumann, S. Bär, and E. Osiac, "Advances in up-conversion lasers based on Er^{3+} and Pr $^{3+}$," *Opt. Mater.*, vol. 26, pp. 365–374, 2004, doi: 10.1016/j.optmat.2003.10.010.

[2] T. V. Gavrilović, D. J. Jovanović, V. Lojpur, and M. D. Dramićanin, "Multifunctional Eu^{3+}- and Er^{3+}/Yb^{3+}-doped $GdVO_4$ nanoparticles synthesized by reverse micelle method," *Sci. Rep.*, vol. 4, 2014, Art. no. 4209, doi: 10.1038/srep04209.

[3] T. Wang, X. Xu, D. Zhou, J. Qiu, and X. Yu, "Red phosphor $Ca_2Ge_7O_{16}$:Eu^{3+} for potential application in field emission displays and white light-emitting diodes," *Mater. Res. Bull.*, vol. 60, pp. 876–881, 2014, doi: 10.1016/j.materresbull.2014.09.091.

[4] L. Y. Zhou, F. Z. Gong, J. X. Shi, M. L. Gong, and H. B. Liang, "A novel red phosphor $Na_2Ca_4Mg_2Si_4O_{15}$:Eu^{3+} for plasma display panels," *Mater. Res. Bull.*, vol. 43, pp. 2295–2299, 2008, doi: 10.1016/j.materresbull.2007.08.014.

[5] Y. Zhang, J. Xu, Q. Cui, and B. Yang, "Eu^{3+} -doped $Bi_4Si_3O_{12}$ red phosphor for solid state lighting: Microwave synthesis, characterization, photoluminescence properties and thermal quenching mechanisms," *Sci. Rep.*, vol. 7, 2017, Art. no. 42464, doi: 10.1038/srep42464.

[6] J. Rajagukguk, R. Situmorang, M. Djamal, and R. Rajaramakrishna, "Structural, spectroscopic and optical gain of Nd^{3+} doped fluorophosphate glasses for solid state laser application," *J. Lumin.*, vol. 216, 2019, Art. no. 116738, doi: 10.1016/j.jlumin.2019.116738.

[7] I. Kumar, A. Kumar, S. Kumar, H. Thakur, N. Dhiman, and A. K. Gathania, "n-UV triggered green emitting Er^{3+} doped Zirconia: A bifunctional material for solid-state lighting and optical thermometry," *Ceramics Int.*, vol. 49, pp. 36979–36987, 2023, doi: 10.1016/j.ceramint.2023.09.030.

[8] C. Kim et al., "Phosphors for plasma display panels," *J. Alloys Compounds*, vol. 311, pp. 33–39, 2000, doi: 10.1016/S0925-8388(00)00856-2.

[9] J. Xue, H. Mi, B. Chun, S. Heum, and J. Hwan, "Dual-functional of non-contact thermometry and field emission displays via efficient $Bi^{3+} \rightarrow Eu^{3+}$ energy transfer in emitting-color tunable $GdNbO_4$ phosphors," *Chem. Eng. J.*, vol. 382, 2020, Art. no. 122861, doi: 10.1016/j.cej.2019.122861.

[10] Z. Xia and A. Meijerink, "Ce^{3+} doped garnet phosphors : Composition modification, luminescence properties and applications," *Chem. Soc. Rev.*, vol. 46, pp. 275–299, 2016, doi: 10.1039/b000000x.

[11] V. Singh et al., "Optik luminescence features of Mn^{2+} -doped Zn_2 SiO_4: A green color emitting phosphor for solid-state lighting," *Optik (Stuttg)*, vol. 225, 2021, Art. no. 165715, doi: 10.1016/j.ijleo.2020.165715.

[12] B. Li et al., "Cyan-emitting $Ba_3Y_2B_6O_{15}$: Ce^{3+}, Tb^{3+} phosphor : A potential color converter for near-UV-excited white LEDs," *J. Lumin.*, vol. 211, pp. 388–393, 2019, doi: 10.1016/j.jlumin.2019.04.001.

[13] Z. J. Jiasong Zhong, D. Chen, W. Zhao, Y. Zhou, H. Yu, and L. Chen, "Garnet-based $Li_6CaLa_2Sb_2O_{12}$:Eu^{3+} red phosphors: A potential color-converting material for warm white light-emitting," *J. Mater. Chem. C.*, vol. 4, pp. 5559–5563, 2016, doi: 10.1039/C6TC01484D.

[14] H. Thakur, A. K. Gathania, I. Kumar, and R. K. Singh, "Tunable white light photoluminescence of a single phase Tm^{3+}/Tb^{3+}/Eu^{3+} codoped $GdPO_4$ phosphor," *Mater. Today Commun.*, vol. 36, 2023, Art. no. 106458, doi: 10.1016/j.mtcomm.2023.106458.

[15] P. Du and J. S. Yu, "Near-ultraviolet light induced visible emissions in Er^{3+}-activated La_2MoO_6 nanoparticles for solid-state lighting and non-contact thermometry," *Chem. Eng. J.*, vol. 327, pp. 109–119, 2017, doi: 10.1016/j.cej.2017.06.069.

[16] I. Kumar, A. Kumar, S. Kumar, H. Thakur, and A. K. Gathania, "Synthesis, structure, and photoluminescence analysis of thermally stable Sm^{3+} doped YPO_4 phosphor," *J. Phys. Conf. Ser.*, vol. 2663, 2023, Art. no. 012002, doi: 10.1088/1742-6596/2663/1/012002.

[17] Y. Zhao, X. Wang, Y. Zhang, Y. Li, and X. Yao, "Optical temperature sensing of up-conversion luminescent materials: Fundamentals and progress," *J. Alloys Compounds*, vol. 817, 2020, Art. no. 152691, doi: 10.1016/j.jallcom.2019.152691.

[18] X. Wang, Q. Liu, Y. Bu, C. S. Liu, and T. Yan, "Optical temperature sensing of rare-earth ion doped phosphors," *RSC Adv.*, vol. 5, pp. 86219–86236, 2015, doi: https://doi.org/10.1039/C5RA16986K.

[19] R. Monika, R. S. Yadav, A. Rai, and S. B. Rai, "NIR light guided enhanced photoluminescence and temperature sensing in Ho^{3+}/Yb^{3+}/Bi^{3+} co-doped $ZnGa_2O_4$ phosphor," *Sci. Rep.*, vol. 11, 2021, Art. no. 4148, doi: 10.1038/s41598-021-83644-9.

[20] F. Men et al., "Thermal-enhanced near-infrared upconversion luminescence of Er^{3+} for high-sensitive optical temperature sensing," *J. Lumin.*, vol. 236, 2021, Art. no. 118153, doi: 10.1016/j.jlumin.2021.118153.

[21] K. Pavani et al., "Analogy of different optical temperature sensing techniques in $LaNbO_4$: Er^{3+} /Yb $^{3+}$ phosphor," *J. Lumin.*, vol. 235, 2021, Art. no. 117992, doi: 10.1016/j.jlumin.2021.117992.

[22] I. Kumar, A. Kumar, S. Kumar, G. B. Nair, H. C. Swart, and A. K. Gathania, "Simultaneous realization of FIR-based multimode optical thermometry and photonic molecular logic gates in Er^{3+} and Yb^{3+} co-doped $SrTiO_3$ phosphor," *Physica Scripta*, vol. 98, 2023, Art. no. 105532, doi: 10.1088/1402-4896/acfa2b.

[23] H. Zhou et al., "Optical temperature sensing properties of Tm^{3+} /Yb^{3+} co-doped LuAG polycrystalline phosphor based on up-conversion luminescence," *J. Lumin.*, vol. 229, 2021, Art. no. 117656, doi: 10.1016/j.jlumin.2020.117656.

[24] D. Wawrzynczyk, A. Bednarkiewicz, M. Nyk, and M. Samoc, "Nanoscale neodymium (III) doped fluoride nanoparticles as non-contact optical," *Nanoscale*, vol. 4, pp. 6959–6961, 2012, doi: 10.1039/c2nr32203j.

[25] H. Thakur, A. K. Gathania, S. Kachhap, S. K. Singh, and R. K. Singh, "Coprecipitation synthesis, structural, optical properties, and thermometry application of Tm^{3+}/Yb^{3+} co-doped YPO_4 phosphor," *J. Lumin.*, vol. 254, 2023, Art. no. 119513, doi: 10.1016/j.jlumin.2022.119513.

[26] K. Li, D. Zhu, and H. Lian, "Up-conversion luminescence and optical temperature sensing properties in novel $KBaY(MoO_4)_3:Yb^{3+}, Er^{3+}$ materials for temperature sensors," *J. Alloys Compounds*, vol. 816, 2020, Art. no. 152554, doi: 10.1016/j.jallcom.2019.152554.

[27] K. Li, D. Zhu, and C. Yue, "Exceptional low-temperature fluorescence sensing properties in novel $KBaY(MoO_4)_3:Yb^{3+}$,Ho^{3+} materials based on FIR of Ho^{3+} transitions $^5F_{5(1)} \rightarrow {}^5I_8/{}^5S_2 \rightarrow {}^5I_8$," *J. Mater. Chem. C.*, vol. 10, pp. 6603–66010, 2022.

[28] I. Kumar and A. K. Gathania, "Photoluminescence and quenching study of the Sm^{3+} doped $LiBaPO_4$ phosphor," *J. Mater. Sci. Mater. Electron.*, vol. 33, pp. 328–341, 2021, doi: 10.1007/s10854-021-07301-7.

[29] A. S. Altowyan et al., "Synthesis and properties of novel $Pb/La/WO_4:Eu^{3+}$ red phosphors for white light emitting diodes (WLEDs)," *Optik (Stuttg)*, vol. 268, 2022, Art. no. 169805, doi: 10.1016/j.ijleo.2022.169805.

[30] W. Wang, S. Song, B. Cao, and J. Li, "Bi^{3+} and Eu^{3+} co-doped $CsPbCl_3$ perovskite quantum dots with efficient controllable blue emission via energy transfer," *J. Lumin.*, vol. 247, 2022, Art. no. 118901, doi: 10.1016/j.jlumin.2022.118901.

[31] P. P. Sukul and H. C. Swart, "Synergistic red dominancy over green up-conversion studies in $PbZrTiO_3:Er^{3+}/Yb^{3+}$ phosphor synthesized via two different modified technique and flexible thin-film thermometer demonstration on C1 : $PbZrTiO_3$ @ P," *J. Alloys Compounds*, vol. 966, 2023, Art. no. 171656, doi: 10.1016/j.jallcom.2023.171656.

[32] E. V. Ushakova, S. A. Cherevkov, V. A. Kuznetsova, and A. V. Baranov, "Lead-free perovskites for lighting and lasing applications: A minireview," *Mater. (Basel)*, vol. 12, pp. 1–27, 2019, doi: 10.3390/ma122333845.

[33] E. Tm et al., "Red, green, blue and bright white upconversion luminescence of $CaTiO_3:Er^{3+}/Tm^{3+}/Yb^{3+}$ nanocrystals," *J. Alloys Compounds*, vol. 541, pp. 505–509, 2012, doi: 10.1016/j.jallcom.2012.07.008.

[34] S. Sasidharan, G. Jyothi, and K. G. Gopchandran, "Solution combustion synthesis and luminescence dynamics of $CaTiO_3$:Eu^{3+}, Y^{3+}," *J. Lumin.*, vol. 235, 2021, Art. no. 118048, doi: 10.1016/j.jlumin.2021.118048.

[35] A. Nag Bhargavi and G. Khare, "Luminescence studies of perovskite structured titanates: A review," *Opt. Spectrosc.*, vol. 118, pp. 902–917, 2015, doi: 10.1134/S0030400X15060156.

[36] H. Mizoguchi, K. Ueda, and M. Orita, "Decomposition of water by a $CaTiO_3$ photocatalyst under UV light irradiation," *Mater. Res. Bull.*, vol. 37, pp. 2401–2406, 2002, doi: 10.1016/S0025-5408(02)00974-1.

[37] X. Xu, Y. Tang, F. Mo, L. Zhou, and B. Li, "Synthesis and luminescent properties of $CaTiO_3:Eu^{3+}$, Al^{3+} phosphors," *Ceram. Int.*, vol. 40, pp. 10887–10892, 2014, doi: 10.1016/j.ceramint.2014.03.083.

[38] J. Mu, J. Liu, and L. Gao, "Upconversion fluorescence modulation of $CaTiO_3:Yb^{3+}/Er^{3+}$ nanocubes via Zn^{2+} introduction," *Optoelctronics Lett.*, vol. 18, pp. 0129–0134, 2022, doi: 10.1007/s11801-022-1125-7.

[39] Y. Pan et al., "Synthesis and red luminescence of Pr^{3+}-doped $CaTiO_3$ nano- phosphor from polymer precursor," *J. Solid State Chem.*, vol. 174, pp. 69–73, 2003, doi: 10.1016/S0022-4596(03)00175-0.

[40] Y. R. Parauha, V. Sahu, and S. J. Dhoble, "Prospective of combustion method for preparation of nanomaterials: A challenge," *Mater. Sci. Eng. B.*, vol. 267, 2021, Art. no. 115054, doi: 10.1016/j.mseb.2021.115054.

[41] S. Thakur and A. K. Gathania, "Investigation of optical properties of YVO_4–Er^{3+} nano-phosphors at different Er^{3+} concentrations and calcination temperatures," *J. Mater. Sci. Mater. Electron.*, vol. 27, pp. 1988–1993, 2016, doi: 10.1007/s10854-015-3982-3.

[42] Y. Wang, C. G. Niu, L. Wang, Y. Wang, X. G. Zhang, and G. M. Zeng, "Synthesis of fern-like $Ag/AgCl/CaTiO_3$ plasmonic photocatalysts and their enhanced visible-light photocatalytic properties," *RSC Adv.*, vol. 6, pp. 47873–47882, 2016, doi: 10.1039/c6ra06435c.

[43] D. Chakrabarty and S. Mahapatra, "Aragonite crystals with unconventional morphologies," *J. Mater. Chem.*, vol. 9, pp. 2953–2957, 1999, doi: 10.1039/A905407C.

[44] D. Meroni, L. Porati, F. Demartin, and D. Poelman, "Sol-gel synthesis of $CaTiO_3:Pr^{3+}$ red phosphors: Tailoring the synthetic parameters for luminescent and afterglow applications," *ACS Omega*, vol. 2, pp. 4972–4981, 2017, doi: 10.1021/acsomega.7b00761.

[45] N. P. Bhagya, P. A. Prashanth, R. Hari, B. M. Nagabhushana, and R. S. Raveendra, "Photoluminescence studies of Eu^{3+} activated $SrTiO_3$ nanophosphor prepared by solution combustion approach," *Opt.-Int. J. Light Electron Opt.*, vol. 145, pp. 678–687, 2017, doi: 10.1016/j.ijleo.2017.07.003.

[46] H. K. Yang et al., "Luminescent characteristics of $CaTiO_3:Pr^{3+}$ thin films prepared by pulsed laser deposition method with various substrates," *Appl. Surf. Sci.*, vol. 255, pp. 5062–5066, 2009, doi: 10.1016/j.apsusc.2008.12.068.

[47] E. Greenberg and R. D. E. Pape, "Energy transfer between fluoride manganese (III) and erbium (III) in various glasses," *J. Solid State Chem.*, vol. 53, pp. 236–245, 1984, doi: 10.1016/0022-4596(84)90097-5.

[48] H. R. Girisha, B. R. Radha krushna, D. R. Lavanya, P. B. Daruka, S. C. Sharma, and H. Nagabhushana, "Anti-counterfeiting, latent fingerprint detection and optical thermometry using a multi-stimulus down-converting $La_2CaZnO_5:Er^{3+}$ phosphor," *Opt. Mater.*, vol. 134, 2022, Art. no. 113053, doi: 10.1016/j.optmat.2022.113053.

[49] I. Kumar, A. Kumar, and A. K. Gathania, "Activation of zirconia nanophosphors with Eu^{3+} to demonstrate multifunctional optical applications," *Mater. Chem. Phys.*, vol. 292, 2022, Art. no. 126846, doi: 10.1016/j.matchemphys.2022.126846.

[50] I. Charak, M. Manhas, A. K. Bedyal, A. Vij, H. C. Swart, and V. Kumar, "Synthesis, luminescence and photometric investigation of $Sr_2B_2O_5:Dy^{3+}$ phosphor for UV-based white LEDs," *Appl. Phys. A.*, vol. 129, 2023, Art. no. 222, doi: 10.1007/s00339-023-06488-2.

[51] P. Sukul, K. Kumar, and H. Swart, "Erbium energy bridging upconversion mechanism studies on $BAKL:Er^{3+}/Yb^{3+}$ glass-ceramics and simultaneous enhancement of color purity of the green luminescence," *Dalton Trans.*, vol. 51, pp. 2827–2839, 2022, doi: 10.1039/D1DT03918K.

[52] Y. Cui et al., "Improving the temperature-sensing performance of the $SrZn_{0.33}Nb_{0.67}O_3:Pr^{3+}$ phosphor via Ga^{3+} doping," *Mater. Adv.*, vol. 3, pp. 3267–3277, 2022, doi: 10.1039/d1ma01247a.

[53] V. Sangwan, M. Jayasimhadri, and D. Haranath, "Colour-tunable and warm white light emitting thermally stable Dy^{3+}/Sm^{3+} co-activated tungstate-tellurite glasses for photonic applications," *J. Lumin.*, vol. 266, 2024, Art. no. 120276, doi: 10.1016/j.jlumin.2023.120276.

[54] P. Du, L. Luo, Q. Yue, and W. Li, "The simultaneous realization of high- and low-temperature thermometry in Er^{3+}/Yb^{3+}-codoped Y_2O_3 nanoparticles," *Mater. Lett.*, vol. 143, pp. 209–211, 2015, doi: 10.1016/j.matlet.2014.12.123.

[55] J. Zhang, Y. Zhang, and X. Jiang, "Investigations on upconversion luminescence of $K_3Y(PO_4)_2:Yb^{3+}$-$Er^{3+}/Ho^{3+}/Tm^{3+}$ phosphors for optical temperature sensing," *J. Alloys Compd.*, vol. 748, pp. 438–445, 2018, doi: 10.1016/j.jallcom.2018.03.127.

[56] W. Ran et al., "Application of thermally coupled energy levels in Er^{3+} doped $CdMoO_4$ phosphors: Enhanced solid-state lighting and non-contact thermometry," *Mater. Res. Bull.*, vol. 117, pp. 63–71, 2019, doi: 10.1016/j.materresbull.2019.04.035.